

Online Research @ Cardiff

This is an Open Access document downloaded from ORCA, Cardiff University's institutional repository: <https://orca.cardiff.ac.uk/id/eprint/114954/>

This is the author's version of a work that was submitted to / accepted for publication.

Citation for final published version:

Jafari, Azadeh, Chitsaz, Alizera, Nouri, Reza and Phillips, Timothy N. ORCID: <https://orcid.org/0000-0001-6455-1205> 2018. Property preserving reformulation of constitutive laws for the conformation tensor. Theoretical and Computational Fluid Dynamics 32 , pp. 789-803. 10.1007/s00162-018-0476-y file

Publishers page: <https://doi.org/10.1007/s00162-018-0476-y>
<<https://doi.org/10.1007/s00162-018-0476-y>>

Please note:

Changes made as a result of publishing processes such as copy-editing, formatting and page numbers may not be reflected in this version. For the definitive version of this publication, please refer to the published source. You are advised to consult the publisher's version if you wish to cite this paper.

This version is being made available in accordance with publisher policies.

See

<http://orca.cf.ac.uk/policies.html> for usage policies. Copyright and moral rights for publications made available in ORCA are retained by the copyright holders.



Property Preserving Reformulation of Constitutive Laws for the Conformation Tensor

Azadeh Jafari · Alireza Chitsaz · Reza Nouri · Timothy N. Phillips

Received: date / Accepted: date

Abstract The challenge for computational rheologists is to develop efficient and stable numerical schemes in order to obtain accurate numerical solutions for the governing equations at values of practical interest of the Weissenberg numbers. This study presents a new approach to preserve the symmetric positive definiteness of the conformation tensor and to bound the magnitude of its eigenvalues. The idea behind this transformation is lies with the matrix logarithm formulation. Under the logarithmic transformation, the eigenvalue spectrum of the new conformation tensor varies from infinite positive to infinite negative. But, reconstruction the classical formulation from unbounded eigenvalues doesn't achieve meaningful results. This enhanced formulation, hyperbolic tangent, prevails the previous numerical failure by bounding the magnitude of eigenvalues in a manner that positive definite is always satisfied. In order to evaluate the capability of the hyperbolic tangent formulation we performed a numerical simulation of FENE-P fluids in a rectangular channel in the context of the finite element method. Under this new transformation, the maximum attainable Weissenberg number increases 21.4% and 112.5% comparing the standard log-conformation and classical constitutive equation respectively.

A. Jafari
School of Mechanical Engineering, College of Engineering, University of Tehran, Tehran,
P.O. Box: 11155-4563, Iran
Tel.: +98-21-61114037
E-mail: azadeh.jafari@ut.ac.ir

R. Nouri
School of Mechanical Engineering, College of Engineering, University of Tehran, Tehran,
P.O. Box: 11155-4563, Iran

A. Chitsaz
School of Mechanical Engineering, College of Engineering, University of Tehran, Tehran,
P.O. Box: 11155-4563, Iran

T.N. Phillips
School of Mathematics, Cardiff University, Cardiff, CF24 4AG, United Kingdom

Keywords Viscoelastic fluid flows · High Weissenberg number problem · Hyperbolic tangent

1 Introduction

It is well known that the conformation tensor should, in principle, remain symmetric positive definite (SPD) as it evolves in time [8]. In fact, this property is crucial for the well-posedness of its evolution equation [12, 4]. Although many constitutive equations have been proven to be Hadamard stable, in practice this property is violated in many numerical simulations. Most likely, this is caused by the accumulation of spatial discretization error that arises from numerical integration of the governing equations. This gives rise to spurious negative eigenvalues, causing the conformation tensor to lose its SPD property and Hadamard instabilities to grow. This was an obstacle to early attempts to numerically simulate viscoelastic fluids [14].

Recently, a logarithm representation of the conformation tensor was proposed by Fattal and Kupferman [5, 6]. The essential idea is based on the conjecture that the high Weissenberg number problem (HWNP) may be caused by the failure of polynomial-based approximations to properly represent exponential profiles developed by the conformation tensor in regions of high strain rate for high Deborah number flows. The deformation term in the constitutive equation is composed of extensional and rotational components. The extensional component under the logarithmic transformation acts additively rather than multiplicatively in the standard formulation. So, the polynomial interpolation can properly capture the steep stress gradient in the logarithmic transformation. This proposed transformation preserves the symmetric positive definiteness of the conformation tensor even at high Weissenberg number for any numerical scheme.

Hulsen et al. [9] first implemented the log conformation formulation in a finite element context, using the DEVSS/DG formulation for the flow around a cylinder for the Oldroyd-B and Giesekus models. Under the logarithm transformation, the maximum attainable Weissenberg number was around 100. However they reported a lack of convergence near the cylinder for the Oldroyd-B model.

Kwon [11] presented an alternative derivation of the tensor logarithmic representation of the differential constitutive equation and provided a numerical example with the Leonov model for the flow through a 4:1 planar contraction using SUPG and SU stabilization techniques. Dramatic improvement of the performance of the computational algorithm with stable convergence was demonstrated. The author achieved converged numerical solutions for $De = 132$ with a coarse mesh and $De = 193$ for a refined mesh. This new formulation can be used only for the few differential constitutive equations that have been proven to be globally stable [13].

Vaithianathan and Collins [17] recently presented two matrix decompositions that guaranteed the construction of a conformation tensor in a manner that

ensures that positive definiteness is always satisfied. In parallel, they also proposed a change of variable in the conformation tensor in order to also enforce the boundness of its trace, as dictated by the constitutive model used (FENE-P). The algorithms were implemented into isotropic turbulence simulations.

A simple alternative form of the log conformation formulation was proposed by Coronado et al. [3]. The flows of Oldroyd-B and Larson-type fluids were simulated for the benchmark problem of flow past a cylinder in a channel using DEVSSS-TG/SUPG methods. The maximum attainable Weissenberg numbers were 1.05 and 12.3, respectively.

Housiadas et al. [7] introduced a different implementation of the log-conformation representation to allow for very accurate spectral approximations and efficient time integration while smoothing the final result explicitly by applying a multi-grid diffusion correction directly to the classical conformation tensor. In order to eradicate numerical errors, they introduced a smoothing operation that removed non-physical instabilities from the numerical approximation.

Jafari et al. [10] showed that although the use of the log conformation tensor can be helpful in preserving the symmetric positive definiteness of the conformation tensor, it is also mandatory for the FENE family of models to satisfy the boundedness of the conformation tensor. In order to remove numerical instabilities a new extended matrix logarithm formulation was developed.

Tomé et al. [16] applied the log formulation for time dependent extrudate swell and jet buckling of UCM fluids. The momentum equation is solved using a finite difference marker-and-cell type method. Their numerical results showed a significant increase in the maximum attainable Weissenberg number for both case studies.

Afonso et al. [1] presented a generic formulation for many transformation rules applicable to conformation tensor models. The kernel-conformation transformation function can include any continuous, invertible and differentiable matrix transformation. In their paper, Afonso et al. [1] considered the linear shifted, logarithmic and k th root functions of the conformation tensor \mathbf{C} and applied the approach to the benchmark problem of flow of an Oldroyd B fluid past a confined cylinder to assess the relative merits of these functions. At low Weissenberg numbers they found that this approach generates results that are consistent with the standard discretization of the conformation tensor. However, the numerical efficiency of this approach at high Weissenberg numbers is highly dependent on the choice of kernel function and the singularities introduced either by physical description of the flow or the choice of constitutive equation.

Saramito [15] proposed a new log-conformation formulation for Johnson-Segalman viscoelastic fluids. In contrast to the formulation of Fattal and Kupferman, this new transformation is non-singular as the Weissenberg number tends to zero. He applied this new formulation to the lid driven cavity in the context of the finite element method using velocity-pressure approximation and discontinuous Galerkin upwind treatment for stress. The numerical results are in good agreement qualitatively with experimental measurements.

Comminal et al. [2] presented a new streamfunction/log-conformation formula-

tion for Oldroyd-B fluids. Regarding the pressureless formulation, the numerical results are free from pressure-velocity decoupling errors, which enhances the robustness and efficiency of the algorithm. Their numerical results at high Wessener number around 5 show quasi-periodic instability at the upstream corner of the moving wall.

The log transformation guarantees the positive eigenvalues of the conformation tensor during numerical simulations. While the action of the symmetric positive definite (SPD) property of the conformation tensor during the simulation is a necessary condition for stable simulations, it is definitely not a sufficient condition to reach meaningful results. Actually, solving the constitutive equation in the new scale, logarithmically, allows the eigenvalues of the new conformation tensor to range over the entire real line from infinite negative to infinite positive values while reconstructing the classical conformation tensor from either infinite positive or infinite negative eigenvalues does not have any physical meaning.

The aim of this paper is the development of a mathematical model to preserve both the SPD of the conformation tensor and also to bound the magnitude of the eigenvalues. The hyperbolic tangent formulation of the constitutive equation removes some of the stiffness associated with the standard form of the constitutive equation. We demonstrate that this has the effect of increasing the critical Weissenberg number, thereby delaying the so-called high Weissenberg number problem.

There are a number of alternative formulations proposed in the literature such as the new extended matrix logarithm formulation [13] and the sequence mapping of Housiadas et al. [12]. These two formulations are based on the log conformation representation for viscoelastic fluids which is designed to preserve symmetric positive definiteness. Both formulations use an additional mapping to ensure that the eigenvalues of the conformation tensor are bounded. In contrast, the hyperbolic tangent formulation proposed in the present article preserves the symmetric positive definiteness and bounds the eigenvalues of the conformation tensor simultaneously. This is a major advantage of the approach described in this paper.

This paper is organized as follows. A new state-of-the-art reformation of the constitutive equation using the hyperbolic tangent tensor is introduced in Section 2. The detailed differential constitutive equation for the hyperbolic tangent tensor in 2D is presented in Section 3. Some numerical results are presented in Section 4 that demonstrate the enhanced stability properties of the new reformulation of the constitutive equation.

2 The state-of-the-art of the hyperbolic tangent tensor

Most differential constitutive models can be written in the following general form:

$$\frac{\partial \mathbf{C}}{\partial t} + (\mathbf{u} \cdot \nabla) \mathbf{C} - (\nabla \mathbf{u})^T \cdot \mathbf{C} - \mathbf{C} \cdot \nabla \mathbf{u} = \frac{1}{W_e} \boldsymbol{\Psi} \quad (1)$$

where \mathbf{C} is the conformation tensor, \mathbf{u} is the velocity field and $\boldsymbol{\Psi}$ is a model-dependent tensor function of \mathbf{C} with coefficients that possibly depend on the invariants of \mathbf{C} or the rate of deformation tensor. For example, the Oldroyd-B model is characterized by $\boldsymbol{\Psi} = \mathbf{I} - \mathbf{C}$, the FENE-CR model by $\boldsymbol{\Psi} = \frac{\mathbf{I} - \mathbf{C}}{1 - \frac{\text{tr}(\mathbf{C})}{b^2}}$ where the parameter b measures the maximum extensibility of the dumbbells, and the FENE-P model by $\boldsymbol{\Psi} = \mathbf{I} - \frac{\mathbf{C}}{1 - \frac{\text{tr}(\mathbf{C})}{b^2}}$.

As explained in the introduction, Fattal and Kupferman [5] proposed a reformulation of classical constitutive equations by introducing a new variable $\mathbf{H} = \ln(\mathbf{C})$ to derive the so-called logarithmic formulation. An important observation is that the logarithm is an isotropic tensor function and so \mathbf{C} and \mathbf{H} possess an identical set of principal axes. This transformation forces the eigenvalues of the conformation tensor to remain positive throughout the simulation. Solving the constitutive equation in the new formulation for the logarithm of the conformation tensor means that the eigenvalues of the new conformation tensor, \mathbf{H} , range over the whole real line $(-\infty, +\infty)$, which enforces the eigenvalues of the classical conformation tensor, \mathbf{C} , to range over the positive semi-infinite interval $[0, +\infty)$ (Fig.1a).

Reconstructing the classical conformation and viscoelastic stress tensors from eigenvalues that are unbounded does not have any physical meaning. A possible remedy which would bound the magnitude of the eigenvalues of \mathbf{C} is to use the hyperbolic tangent of \mathbf{H} (Fig.1b). As is obvious from this figure, however, the variation of the eigenvalues of \mathbf{H} is in the interval $(-\infty, +\infty)$, while the eigenvalues of \mathbf{C} are totally bounded and contained in the interval $[-1, +1]$. To preserve the symmetric positive definiteness of the conformation tensor, it is mandatory to ensure that the eigenvalues of the conformation tensor, \mathbf{C} , are non-negative. To do so, we use the enhanced formulation of hyperbolic tangent of the conformation tensor. We transform the classical constitutive equation based on the conformation tensor, \mathbf{C} , to a new one based on the tensor \mathbf{H} , where \mathbf{C} and \mathbf{H} are related by:

$$\mathbf{C} = M(\tanh(\mathbf{H}) + \mathbf{I}) \quad (2)$$

or:

$$\mathbf{C} = 2M \frac{e^{\mathbf{H}}}{e^{\mathbf{H}} + e^{-\mathbf{H}}} \quad (3)$$

where M is a constant that is model-dependent. For example, for the FENE family, the square of the corresponding finite extensibility parameter of the polymer must be an upper limit for the trace of the conformation tensor. So M should be chosen in some way to satisfy this condition ($M \geq \frac{b^2}{2}$). This new formulation preserves both the SPD of the conformation tensor and also bounds the magnitude of the eigenvalues of \mathbf{C} . Any function of a positive definite matrix is by definition an isotropic function of the original tensor. Therefore \mathbf{C} and \mathbf{H} have a common set of eigenvectors.

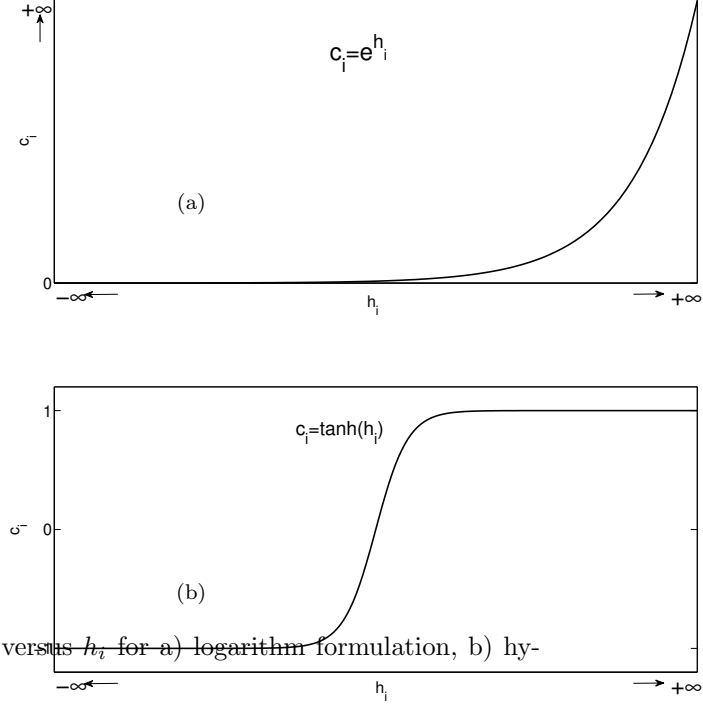


Fig. 1: Typical variation of c_i versus h_i for a) logarithm formulation, b) hyperbolic tangent formulation.

3 Hyperbolic Tangent Formulation of the Constitutive Equation

In this study, we follow the approach adopted by Kwon [11] for deriving the evolution equations. In the case of 2D planar flow, and adopting the same notation as Kwon, the eigenvalue problem for the conformation tensor \mathbf{H} in the continuous domain yields the eigenvalues:

$$h_1 = \frac{1}{2} \left[h_{11} + h_{22} + \sqrt{(h_{11} - h_{22})^2 + 4h_{12}^2} \right] \quad (4)$$

$$h_2 = \frac{1}{2} \left[h_{11} + h_{22} - \sqrt{(h_{11} - h_{22})^2 + 4h_{12}^2} \right] \quad (5)$$

The eigenvectors of \mathbf{H} are written in the form:

$$\mathbf{n}_1 = \begin{bmatrix} n_1 \\ n_2 \end{bmatrix} \quad \text{and} \quad \mathbf{n}_2 = \begin{bmatrix} -n_2 \\ n_1 \end{bmatrix} \quad (6)$$

with $n_1^2 + n_2^2 = 1$. The components of the eigenvectors can be determined by solving the characteristic equation for \mathbf{H} :

$$n_1^2 = \frac{h_{12}^2}{(h_1 - h_{11})^2 + h_{12}^2} \quad (7)$$

$$n_2^2 = \frac{(h_1 - h_{11})^2}{(h_1 - h_{11})^2 + h_{12}^2} \quad (8)$$

$$n_1 n_2 = \frac{h_{12}(h_1 - h_{11})}{(h_1 - h_{11})^2 + h_{12}^2} \quad (9)$$

201 The characteristic equation for \mathbf{C} is written as:

$$\mathbf{C} \cdot \mathbf{n}_i = c_i \mathbf{n}_i \quad (10)$$

202 Differentiation of the above equation with respect to time yields:

$$\dot{\mathbf{C}} \cdot \mathbf{n}_i + \mathbf{C} \cdot \dot{\mathbf{n}}_i = \dot{c}_i \mathbf{n}_i + c_i \dot{\mathbf{n}}_i \quad (11)$$

203 Then taking the scalar product with another eigenvector yields the following
204 result:

$$\begin{aligned} \mathbf{n}_j \cdot \dot{\mathbf{C}} \cdot \mathbf{n}_i &= \mathbf{n}_j \cdot (\dot{c}_i \mathbf{n}_i) + \mathbf{n}_j \cdot (c_i \dot{\mathbf{n}}_i) - \mathbf{n}_j \cdot (\mathbf{C} \cdot \dot{\mathbf{n}}_i) \\ &= \dot{c}_i \delta_{ij} + (c_i - c_j) \dot{\mathbf{n}}_i \cdot \mathbf{n}_j \end{aligned} \quad (12)$$

205 from which we deduce:

$$\begin{aligned} i) \quad \dot{c}_i &= \mathbf{n}_i \cdot \dot{\mathbf{C}} \cdot \mathbf{n}_i & \text{when } i = j \\ ii) \quad \dot{\mathbf{n}}_i \cdot \mathbf{n}_j &= \frac{1}{c_i - c_j} \mathbf{n}_j \cdot \dot{\mathbf{C}} \cdot \mathbf{n}_i & \text{when } i \neq j \end{aligned} \quad (13)$$

206 Due to the isotropic function relation, \mathbf{C} and \mathbf{H} have the same set of eigen-
207 vectors. For the \mathbf{H} -tensor, an equivalent relation is readily obtained as:

$$\mathbf{n}_j \cdot \dot{\mathbf{H}} \cdot \mathbf{n}_i = \dot{h}_i \delta_{ij} + (h_i - h_j) \dot{\mathbf{n}}_i \cdot \mathbf{n}_j \quad (14)$$

208 Introducing $h_i = \frac{1}{2} \ln(\frac{c_i}{2M - c_i})$ so that $\dot{h}_i = M \frac{\dot{c}_i}{c_i(2M - c_i)}$, and combining Eqs.
209 (13) and (14), one obtains:

$$\begin{aligned} i) \quad \mathbf{n}_i \cdot \dot{\mathbf{H}} \cdot \mathbf{n}_i &= M \frac{\dot{c}_i}{c_i(2M - c_i)} = \frac{M}{c_i(2M - c_i)} \mathbf{n}_i \cdot \dot{\mathbf{C}} \cdot \mathbf{n}_i & \text{when } i = j \\ ii) \quad \mathbf{n}_i \cdot \dot{\mathbf{H}} \cdot \mathbf{n}_j &= (h_j - h_i) \dot{\mathbf{n}}_j \cdot \mathbf{n}_i = \frac{h_i - h_j}{c_i - c_j} \mathbf{n}_i \cdot \dot{\mathbf{C}} \cdot \mathbf{n}_j & \text{when } i \neq j \end{aligned} \quad (15)$$

210 In the 2D case Eq. (15) yields:

$$A \begin{pmatrix} \dot{H}_{11} \\ \dot{H}_{12} \\ \dot{H}_{22} \end{pmatrix} = B \quad (16)$$

where A is defined by:

$$A = \begin{pmatrix} n_1^2 & 2n_1n_2 & n_2^2 \\ n_2^2 & -2n_1n_2 & n_1^2 \\ -n_1n_2 & (n_1^2 - n_2^2) & n_1n_2 \end{pmatrix} \quad (17)$$

and B by:

$$B = \begin{pmatrix} \frac{M}{c_1(2M-c_1)}(n_1^2\dot{C}_{11} + 2n_1n_2\dot{C}_{12} + n_2^2\dot{C}_{22}) \\ \frac{M}{c_2(2M-c_2)}(n_2^2\dot{C}_{11} - 2n_1n_2\dot{C}_{12} + n_1^2\dot{C}_{22}) \\ \frac{h_1-h_2}{c_1-c_2}(-n_1n_2\dot{C}_{11} + (n_1^2 - n_2^2)\dot{C}_{12} + n_1n_2\dot{C}_{22}) \end{pmatrix} \quad (18)$$

Multiplying both sides of Eq. (16) by A^{-1} one obtains the evolution equation for the components of \mathbf{H} :

$$\begin{aligned} \dot{H}_{11} &= \left(\frac{M}{c_1(2M-c_1)}n_1^4 + \frac{M}{c_2(2M-c_2)}n_2^4 + 2n_1^2n_2^2\frac{h_1-h_2}{c_1-c_2} \right) \dot{C}_{11} \\ &+ \left(\frac{M}{c_1(2M-c_1)}2n_1^3n_2 - \frac{M}{c_2(2M-c_2)}2n_1n_2^3 - 2n_1n_2(n_1^2 - n_2^2)\frac{h_1-h_2}{c_1-c_2} \right) \dot{C}_{12} \\ &+ \left(\frac{M}{c_1(2M-c_1)}n_1^2n_2^2 + \frac{M}{c_2(2M-c_2)}n_1^2n_2^2 - 2n_1^2n_2^2\frac{h_1-h_2}{c_1-c_2} \right) \dot{C}_{22} \\ &= G_{11}\dot{C}_{11} + G_{12}\dot{C}_{12} + G_{13}\dot{C}_{22} \end{aligned} \quad (19)$$

$$\begin{aligned} \dot{H}_{12} &= \left(\frac{M}{c_1(2M-c_1)}n_1^3n_2 - \frac{M}{c_2(2M-c_2)}n_1n_2^3 - n_1n_2(n_1^2 - n_2^2)\frac{h_1-h_2}{c_1-c_2} \right) \dot{C}_{11} \\ &+ \left(\frac{M}{c_1(2M-c_1)}2n_1^2n_2^2 + \frac{M}{c_2(2M-c_2)}2n_1^2n_2^2 + (n_1^2 - n_2^2)^2\frac{h_1-h_2}{c_1-c_2} \right) \dot{C}_{12} \\ &+ \left(\frac{M}{c_1(2M-c_1)}n_1n_2^3 - \frac{M}{c_2(2M-c_2)}n_1^3n_2 + n_1n_2(n_1^2 - n_2^2)\frac{h_1-h_2}{c_1-c_2} \right) \dot{C}_{22} \\ &= G_{21}\dot{C}_{11} + G_{22}\dot{C}_{12} + G_{23}\dot{C}_{22} \end{aligned} \quad (20)$$

$$\begin{aligned}
\dot{H}_{22} = & \left(\frac{M}{c_1(2M-c_1)} n_1^2 n_2^2 + \frac{M}{c_2(2M-c_2)} n_1^2 n_2^2 - 2n_1^2 n_2^2 \frac{h_1-h_2}{c_1-c_2} \right) \dot{C}_{11} \\
& + \left(\frac{M}{c_1(2M-c_1)} 2n_1 n_2^3 - \frac{M}{c_2(2M-c_2)} 2n_1^3 n_2 + 2n_1 n_2 (n_1^2 - n_2^2) \frac{h_1-h_2}{c_1-c_2} \right) \dot{C}_{12} \\
& + \left(\frac{M}{c_1(2M-c_1)} n_2^4 + \frac{M}{c_2(2M-c_2)} n_1^4 + 2n_1^2 n_2^2 \frac{h_1-h_2}{c_1-c_2} \right) \dot{C}_{22} \\
= & G_{31} \dot{C}_{11} + G_{32} \dot{C}_{12} + G_{33} \dot{C}_{22}
\end{aligned} \tag{21}$$

where \dot{H}_{ij} and \dot{C}_{ij} are the components of the material time derivative of the corresponding matrices which can be expressed by:

$$\dot{\mathbf{H}} = \frac{\partial \mathbf{H}}{\partial t} + (\mathbf{u} \cdot \nabla) \mathbf{H} \tag{22}$$

$$\dot{\mathbf{C}} = \frac{\partial \mathbf{C}}{\partial t} + (\mathbf{u} \cdot \nabla) \mathbf{C} \tag{23}$$

The above system of equations (19)-(21) can be summarized as:

$$\begin{pmatrix} \dot{H}_{11} \\ \dot{H}_{12} \\ \dot{H}_{22} \end{pmatrix} = \begin{pmatrix} G_{11} & G_{12} & G_{13} \\ G_{21} & G_{22} & G_{23} \\ G_{31} & G_{32} & G_{33} \end{pmatrix} \begin{pmatrix} \dot{C}_{11} \\ \dot{C}_{12} \\ \dot{C}_{22} \end{pmatrix} \tag{24}$$

If we substitute Eq. (22) and (23) in Eq. (24), we get the following equation:

$$\frac{\partial \mathbf{H}}{\partial t} + (\mathbf{u} \cdot \nabla) \mathbf{H} = \begin{pmatrix} G_{11} & G_{12} & G_{13} \\ G_{21} & G_{22} & G_{23} \\ G_{31} & G_{32} & G_{33} \end{pmatrix} \left(\frac{\partial \mathbf{C}}{\partial t} + (\mathbf{u} \cdot \nabla) \mathbf{C} \right) \tag{25}$$

4 Numerical Validation

In order to validate the proposed formulation, we compared the hyperbolic tangent conformation formulation for FENE-P fluids with the classical and logarithmic conformation formulations. To achieve this purpose, numerical simulations in a 2D rectangular channel were performed. The computational domain is shown in Fig. 2.

In this section, we use the centerline velocity, U_{max} , as the characteristic flow speed, the channel width, D , as the length scale, the time scale $\frac{D}{U_{max}}$, the reference pressure ρU_{max}^2 and $\frac{\mu_t U_{max}}{D}$ as the characteristic polymeric stress tensor. The total viscosity of the flow can be defined as $\mu_t = \mu_s + \mu_p$ where μ_s is the solvent viscosity and μ_p is the additional viscosity due to the polymer.

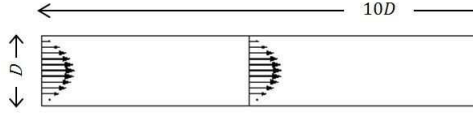


Fig. 2: Computational domain

Subsequently, R_n is introduced as the ratio between solvent viscosity and total viscosity. The Reynolds number is defined as $Re = \rho D U_{max} / \mu_t$. The governing equations in dimensionless form are as follows:

$$\nabla \cdot \mathbf{u} = 0 \quad (26)$$

$$\frac{D\mathbf{u}}{Dt} = -\nabla p + \frac{R_n}{Re} \nabla^2 \mathbf{u} + \frac{1-R_n}{Re} \nabla \cdot \frac{\boldsymbol{\tau}_p}{We} \quad (27)$$

$$\boldsymbol{\tau}_p = \frac{\mathbf{C}}{1 - \frac{\text{tr}(\mathbf{C})}{b^2}} - \mathbf{I} \quad (28)$$

$$\frac{\partial \mathbf{C}}{\partial t} + (\mathbf{u} \cdot \nabla) \mathbf{C} - (\nabla \mathbf{u})^T \cdot \mathbf{C} - \mathbf{C} \cdot (\nabla \mathbf{u}) = - \frac{\boldsymbol{\tau}_p}{We} \quad (29)$$

Eq.(28) states the relationship between the polymeric stress and conformation (\mathbf{C}) tensors for the FENE-P model. In the kernel conformation framework the evolution equation for the hyperbolic tangent tensor H is

$$\begin{aligned} \frac{D\mathbf{H}}{Dt} - \boldsymbol{\Omega} \mathbf{H} - \mathbf{H} \boldsymbol{\Omega} + 2B(\tanh(\mathbf{H}) - \mathbf{I})^{-1} &= \frac{1}{We} \left[\frac{\cosh^2(H)}{M} \right. \\ &\left. - \frac{1}{1 - \frac{\text{tr}(M(\tanh(\mathbf{H}) + \mathbf{I}))}{b^2}} \frac{(I + e^{2H})}{2} \right] \end{aligned} \quad (30)$$

where $\boldsymbol{\Omega}$ is an anti-symmetric pure rotation component of velocity gradient, and B is a symmetric traceless pure extension component of velocity gradient. We consider $Re = 1$ and $R_n = 0.1$ and $b = \sqrt{60}$.

Since constitutive equations are hyperbolic partial differential equations, we merely need to impose the stress at inlet for Eq. (29). Dirichlet Boundary conditions from semi-analytical solution of governing equation are imposed for velocity and viscoelastic stress at inlet (the semi-analytical solution is derived in Appendix A). Open boundary conditions for velocity and viscoelastic stress with zero pressure field are applied at outflow. Initial conditions can affect the numerical results significantly. Consequently, we implement identical initial conditions for each method. For velocity, pressure and conformation tensor (\mathbf{C}), we implement zero initial conditions.

Finally, we implement the finite element method to compute an approximation to the governing equations. All numerical simulations in this section are based on $\Delta t = 10^{-3}$. In order to demonstrate the strength of each formulation, numerical simulations were performed under analogous conditions. In order to use an optimal number of elements, we investigate the dependence of the

outlet velocity on the number of finite elements used in the discretization. Several meshes were considered with 110, 230, 720, 1380, 5600, and 67200 quadrilateral elements and the results from the mesh convergence study are shown in Fig. 3. On more refined meshes, the computation time is increased, while the variations of outlet velocity are less than 1%. Therefore, all remaining computations were performed with 1380 elements, using linear interpolation for the pressure and quadratic interpolation for the velocity and conformation tensor.

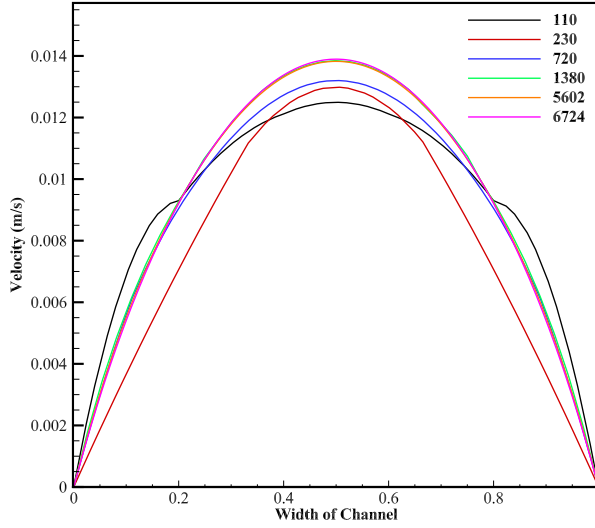


Fig. 3: Typical variation of outflow velocity with different number of elements

5 Results and discussion

In order to validate our numerical simulations, we compare the classical and hyperbolic tangent formulation results with the analytical solution of the Oldroyd-B model (the approach to derive the analytical solution is explained in Appendix B). The velocity and shear stress components at the outflow are selected as the criteria for the validation.

Fig. 4 illustrates agreement between numerical results and analytical solution, then validating our simulations.

As discussed in previous sections, instability of viscoelastic flow grows as the Weissenberg number is increased. In order to illustrate this fact we monitor the relative error for the first normal viscoelastic stress τ_{xx} , $\frac{\|\tau_{xx}^n - \tau_{xx}^{n-1}\|}{\|\tau_{xx}^{n-1}\|}$.

Fig.5 depicts the relative error of the first normal viscoelastic stress for the hyperbolic tangent, classical and logarithmic formulations. Instabilities in the

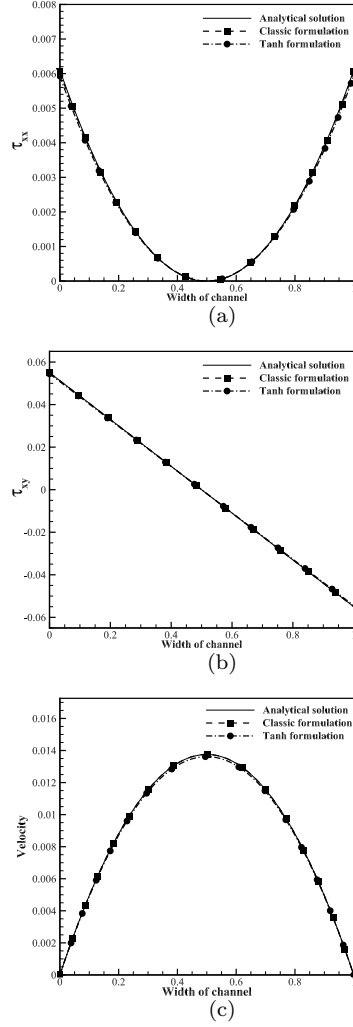


Fig. 4: Comparison for classical and hyperbolic tangent formulation simulations with the analytical solution of a) normal stress, τ_{xx} , b) shear stress, τ_{xy} and c) horizontal velocity for $We=1$, $Re=1$, and $\frac{\partial \mathbf{p}}{\partial x} = -0.11$.

classical, logarithmic, and hyperbolic tangent formulations manifest exponential increase around Weissenberg number 39, 68 and 80, respectively. Hence, we are able to argue that, for planar channel flow, the hyperbolic tangent formulation can achieve higher Weissenberg numbers under analogous conditions. According to Eq. (28) when $\text{tr}(\mathbf{C})$ approaches b^2 , the polymeric stress tensor becomes unbounded and this causes instability in the computation. Therefore, $\text{tr}(\mathbf{C})$ plays an important role in the stability of the numerical simulation. Fig.6 shows the time evolution of $\text{tr}(\mathbf{C})$ for the classical, logarithmic, and hyperbolic

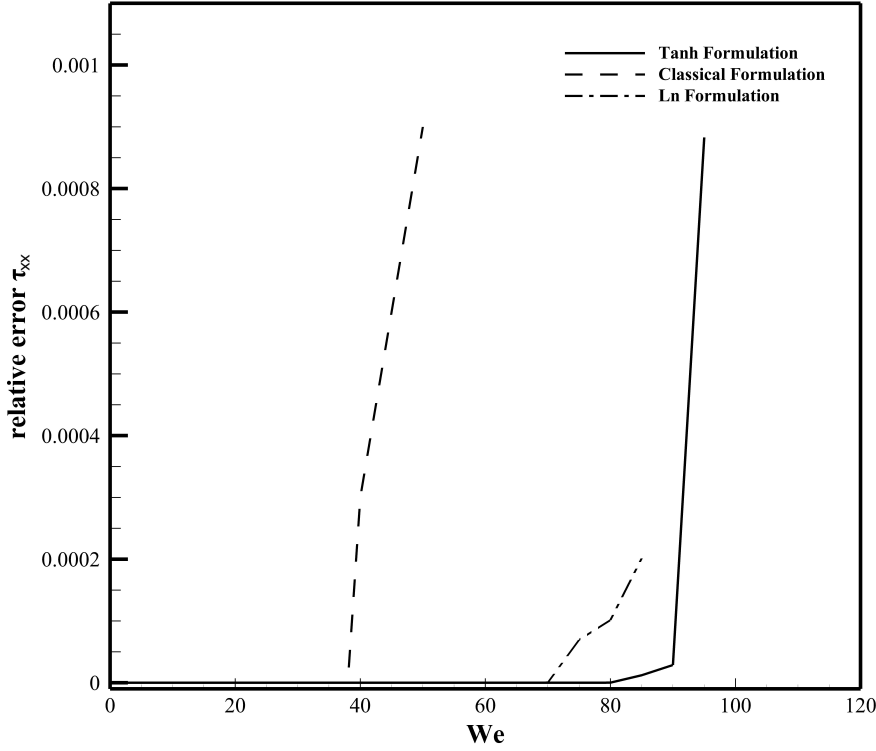


Fig. 5: Typical variation of the relative error for τ_{xx} versus the Weissenberg number

tangent formulations at Weissenberg number 39, 68 and 80, respectively (the critical Weissenberg numbers for each formulation, respectively). For the classical and logarithmic formulations, $\text{tr}(\mathbf{C})$ manifests exponential increase and reaches its critical value of 60, the critical quantity of $\text{tr}(\mathbf{C})$, at time steps 500 and 3000, respectively. After these time steps, the classical and logarithmic formulations become unstable since the polymeric stress tensor becomes unbounded. However, the hyperbolic tangent formulation remains stable at the critical Weissenberg number of 80. Hence, we are able to claim that the instability of the hyperbolic tangent conformation is not due to $\text{tr}(\mathbf{C})$ and accumulation error may be the cause of instability in this formulation.

Fig.7 shows the onset of instability for the hyperbolic tangent conformation at the critical Weissenberg number, $We = 80$, at different time steps. The computation at this Weissenberg number becomes unstable and terminates at the 4523th time step. In Fig.7a, which depicts the flow at 10th time step, we do not observe any instability in the simulation. However, as time proceeds, the instability grows in the flow which can be perceived at 3500th time step

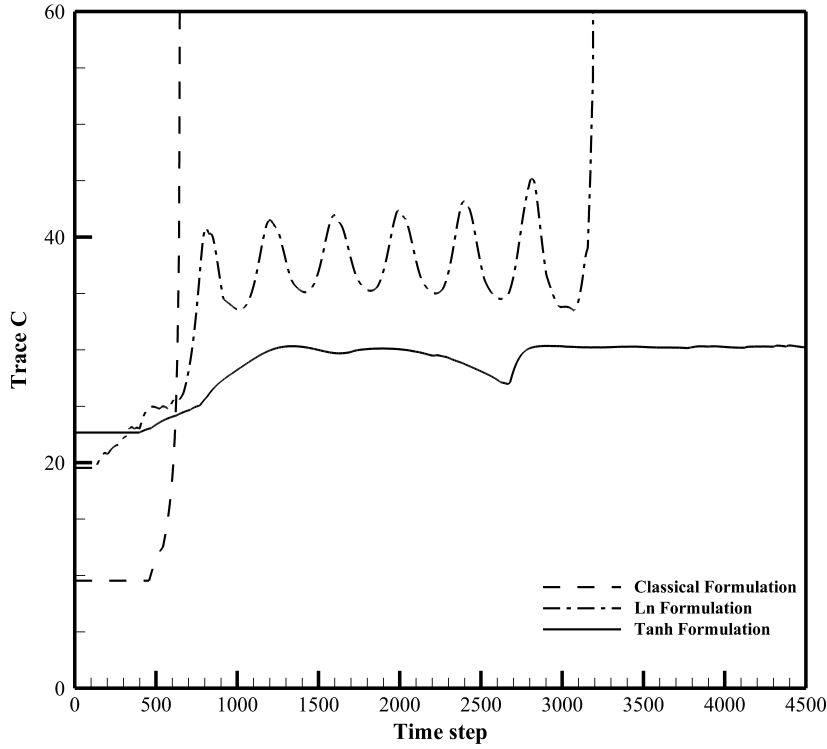


Fig. 6: Evolution of $\text{tr}(\mathbf{C})$ at the critical Weissenberg number

Table 1: Weissenberg limitation values at distinct polynomial orders

Velocity polynomial order	pressure polynomial order	conformation tensor polynomial order	Relative error at $We = 1$	Relative error at $We = 10$
quadratic	linear	quadratic	3.422e-12	1.224e-10
quadratic	linear	cubic	6.423e-13	9.107e-11
quadratic	linear	quartic	5.561e-09	6.543e-07
quadratic	linear	quintic	∞	∞
cubic	quadratic	cubic	9.423e-13	1.102e-11
cubic	quadratic	quartic	5.322e-13	8.651e-12
cubic	quadratic	quintic	6.423e-11	9.330e-08
cubic	quadratic	sextic	2.530e-07	∞
cubic	quadratic	septic	∞	∞

in Fig.7b. Finally, we observe the most instability in the flow at 4523th time step (last time step), which has been caused by accumulation errors, in Fig.7c. In order to investigate the effect of polynomial orders on the numerical simulation, we consider the efficiency of the numerical method with respect to relative error of the first normal viscoelastic stress τ_{xx} . We investigate the performance of two choices of mixed finite element spaces: linear interpolation

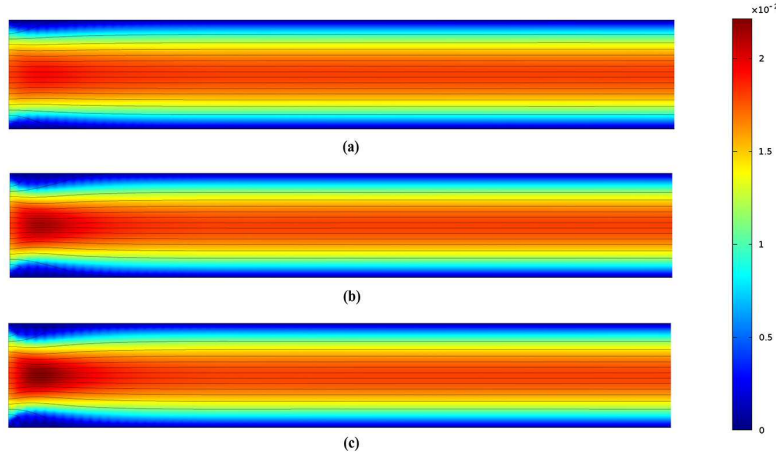


Fig. 7: Velocity fields at $We=80$ at $t = n\Delta t$. a) $n = 10$ b) $n = 3500$ c) $n = 4523$ (Last time step)

for the pressure and quadratic interpolation for the velocity with various interpolations for the conformation tensor (quadratic, cubic, quartic and quintic interpolations); quadratic interpolation for the pressure and cubic interpolation for the velocity with different interpolations for the conformation tensor (cubic, quartic, quintic, sextic and septic interpolations). For the first choice, as can be seen from first 4 rows of Table 1, the capability of hyperbolic tangent formulations to tackle higher Weissenberg numbers initially improves by increasing the order of interpolation for the conformation tensor from quadratic to cubic. However, increasing the order of interpolation for the conformation tensor larger than cubic causes instabilities and the method is not able to reach high Weissenberg numbers. The last five rows of Table 1 illustrates the second choice. Analogous to the first category, initially, enhancing the order of interpolation results in higher accuracy. However, precision declines when the order of interpolation for the conformation tensor is increased to be more than quartic. Increasing the order of interpolation for velocity and pressure from quadratic and linear to cubic and quadratic results in greater accuracy, as lower relative errors are observed in the second category. Since the relative errors at $We = 1$ are lower than the errors at $We = 10$, we can claim that the Weissenberg number is an important factor in the accuracy of the simulation. For a given choice of velocity and pressure approximation spaces the optimum choice of conformation tensor approximation is one order greater than the velocity space.

6 Conclusions

In this study a new mathematical formulation of viscoelastic constitutive equations, the hyperbolic tangent formulation, which preserves both the symmetric positive definiteness of the conformation tensor and bounds the magnitude of its eigenvalues, is proposed. This new formulation has two important features. First of all, it forces the eigenvalues of the conformation tensor to remain positive throughout the simulation. Secondly, reconstruction of the classical conformation tensor from the evolution equations does not encounter the problems associated with the matrix logarithm formulation. In addition, we performed a numerical simulation of viscoelastic flow in a 2D rectangular channel to investigate the performance of the hyperbolic tangent formulation. Results illustrate the advantage of the new formulation over the classical and logarithmic formulations in 2D planar channel, since the hyperbolic tangent formulation attains higher Weissenberg numbers under the same conditions.

Finally, the extension of the approach described in this paper to general 3D flows is entirely possible. Although this is computationally demanding since it requires the calculation of eigenvectors for 3D problems, the computational overhead is not significantly different than for other formulations. The extension to 3D flows will form the basis of future research.

Acknowledgements This research was funded by a Swiss National Science Foundation grant (No. 135676) whose support is gratefully acknowledged.

Appendix A

For fully developed channel flow, Eq. (29) simplifies to:

$$(\nabla \mathbf{u})^T \cdot \mathbf{C} + \mathbf{C} \cdot (\nabla \mathbf{u}) = \frac{\boldsymbol{\tau}_p}{We} \quad (\text{A.1})$$

Hence

$$\tau_{xx} = 2We C_{xy} \frac{\partial u}{\partial y} \quad (\text{A.2})$$

$$\tau_{xy} = We C_{yy} \frac{\partial u}{\partial y} \quad (\text{A.3})$$

$$\tau_{yy} = 0 \quad (\text{A.4})$$

Furthermore, under these conditions Eq. (27) becomes:

$$\nabla p = \frac{R_n}{Re} \nabla^2 \mathbf{u} + \frac{1-R_n}{Re} \nabla \cdot \frac{\boldsymbol{\tau}_p}{We} \quad (\text{A.5})$$

so we obtain

$$\frac{\partial p}{\partial x} = \frac{R_n}{Re} \frac{\partial^2 u}{\partial y^2} + \frac{1}{We} \frac{1-R_n}{Re} \frac{\partial \tau_{xy}}{\partial y} = \text{Const} \quad (\text{A.6})$$

$$\frac{\partial p}{\partial y} = 0 \quad (\text{A.7})$$

By integrating Eq. (A.6) and applying boundary condition at centerline of the channel, we obtain:

$$\frac{\partial u}{\partial y} = -\frac{1}{We} \frac{1-R_n}{R_n} \tau_{xy} + \frac{Re \frac{\partial p}{\partial x}}{R_n} y - \frac{Re \frac{\partial p}{\partial x}}{2R_n} \quad (\text{A.8})$$

Hence, considering Eq. (A.3), we conclude:

$$\frac{\partial u}{\partial y} = \left(\frac{R_n}{R_n + C_{yy} - R_n C_{yy}} \right) \left(\frac{Re \frac{\partial p}{\partial x}}{R_n} y - \frac{Re \frac{\partial p}{\partial x}}{2R_n} \right) \quad (\text{A.9})$$

According to FENE-P model, Eq (28) and Eq. (A.2) to Eq. (A.4), following linear system of equations is obtained:

$$C_{yy} = \frac{b^2 - C_{xx}}{1 + b^2} \quad (\text{A.10})$$

$$C_{xy} = We C_{yy}^2 \frac{\partial u}{\partial y} \quad (\text{A.11})$$

$$C_{xx} = 2We^2 C_{yy}^3 \left(\frac{\partial u}{\partial y} \right)^2 + C_{yy} \quad (\text{A.12})$$

Employing Eq. (A.9), we solve this linear system to find the stress components under fully developed conditions. Furthermore, by integrating Eq. (A.8), the velocity of the flow is given by:

$$u = -\frac{1-R_n}{R_n} \int \frac{\tau_{xy}}{We} dy + \frac{Re \frac{\partial p}{\partial x}}{R_n} y^2 - \frac{Re \frac{\partial p}{\partial x}}{2R_n} y \quad (\text{A.13})$$

Appendix B

In order to find analytical solution of Oldroyd-B model, we consider fully developed condition. Hence, we employed the conformation and momentum equations in fully developed condition from appendix A. According to the Oldroyd-B model, stress components can be written as:

$$\tau_{xx} = \frac{C_{xx} - 1}{We} \quad (B.1)$$

$$\tau_{xy} = \frac{C_{xy}}{We} \quad (B.2)$$

$$\tau_{yy} = \frac{C_{yy} - 1}{We} \quad (B.3)$$

Considering Eqs. (A.2) to (A.4), components of conformation tensor are given by:

$$C_{xx} = 1 + 2We^4 \left(\frac{\partial u}{\partial y} \right)^2 \quad (B.4)$$

$$C_{xy} = We^2 \left(\frac{\partial u}{\partial y} \right) \quad (B.5)$$

$$C_{yy} = 1 \quad (B.6)$$

By inserting the value of C_{yy} to Eq. (A.9), we obtain:

$$\frac{\partial u}{\partial y} = Re \frac{\partial p}{\partial x} \left(y - \frac{1}{2} \right) \quad (B.7)$$

By integrating from Eq. (B.7), the velocity profile can be defined as:

$$u = Re \frac{\partial p}{\partial x} \left(\frac{y^2}{2} - \frac{y}{2} \right) \quad (B.8)$$

Finally, the stress tensor components can be obtained by combining Eqs. (B.1), (B.2) and (B.7)

$$\tau_{xx} = 2We^3 Re^2 \left(\frac{\partial p}{\partial x} \right)^2 \left(y - \frac{1}{2} \right)^2 \quad (B.9)$$

$$\tau_{xy} = We Re \frac{\partial p}{\partial x} \left(y - \frac{1}{2} \right) \quad (B.10)$$

Appendix C

In order to calculate the components (H_{11} , H_{12} and H_{22}) of the tensor \mathbf{H} , we determine the eigenvalues (h_1 and h_2) and the components of eigenvectors (n_1 and n_2) of \mathbf{H} by solving equations (C.1) to (C.5)

$$h_1 = \frac{1}{2} \left[h_{11} + h_{22} + \sqrt{(h_{11} - h_{22})^2 + 4h_{12}^2} \right] \quad (\text{C.1})$$

$$h_2 = \frac{1}{2} \left[h_{11} + h_{22} - \sqrt{(h_{11} - h_{22})^2 + 4h_{12}^2} \right] \quad (\text{C.2})$$

$$n_1^2 = \frac{h_{12}^2}{(h_1 - h_{11})^2 + h_{12}^2} \quad (\text{C.3})$$

$$n_2^2 = \frac{(h_1 - h_{11})^2}{(h_1 - h_{11})^2 + h_{12}^2} \quad (\text{C.4})$$

$$n_1 n_2 = \frac{h_{12}(h_1 - h_{11})}{(h_1 - h_{11})^2 + h_{12}^2} \quad (\text{C.5})$$

Then, by solving the characteristic equations of \mathbf{C} and \mathbf{H} , the relation between eigenvalues of \mathbf{H} and \mathbf{C} is derived (the approach is explained in Appendix A):

$$c_i = \frac{2Me^{2h_i}}{1 + e^{2h_i}} \quad (\text{C.6})$$

According to the characteristic equation for \mathbf{C} , the components are written in the form:

$$c_{11} = n_1^2 c_1 + n_2^2 c_2 \quad (\text{C.7})$$

$$c_{12} = n_1 n_2 (c_1 - c_2) \quad (\text{C.8})$$

$$c_{22} = n_2^2 c_1 + n_1^2 c_2 \quad (\text{C.9})$$

Using equation (C.6), the components of \mathbf{C} are defined by:

$$c_{11} = n_1^2 \frac{2Me^{2h_1}}{1 + e^{2h_1}} + n_2^2 \frac{2Me^{2h_2}}{1 + e^{2h_2}} \quad (\text{C.10})$$

$$c_{12} = n_1 n_2 \left(\frac{2Me^{2h_1}}{1 + e^{2h_1}} - \frac{2Me^{2h_2}}{1 + e^{2h_2}} \right) \quad (\text{C.11})$$

$$c_{22} = n_2^2 \frac{2Me^{2h_1}}{1 + e^{2h_1}} + n_1^2 \frac{2Me^{2h_2}}{1 + e^{2h_2}} \quad (\text{C.12})$$

According to the equations (C.1)-(C.5), the components of \mathbf{C} are derived from the components of \mathbf{H} . Due to Eqs. (19)-(21) the material derivative of \mathbf{H} is

determined as follows:

$$\begin{aligned}
\dot{H}_{11} = & \left(\frac{M}{c_1(2M-c_1)} n_1^4 + \frac{M}{c_2(2M-c_2)} n_2^4 + 2n_1^2 n_2^2 \frac{h_1-h_2}{c_1-c_2} \right) \dot{C}_{11} \\
& + \left(\frac{M}{c_1(2M-c_1)} 2n_1^3 n_2 - \frac{M}{c_2(2M-c_2)} 2n_1 n_2^3 - 2n_1 n_2 (n_1^2 - n_2^2) \frac{h_1-h_2}{c_1-c_2} \right) \dot{C}_{12} \\
& + \left(\frac{M}{c_1(2M-c_1)} n_1^2 n_2^2 + \frac{M}{c_2(2M-c_2)} n_1^2 n_2^2 - 2n_1^2 n_2^2 \frac{h_1-h_2}{c_1-c_2} \right) \dot{C}_{22} \\
= & G_{11} \dot{C}_{11} + G_{12} \dot{C}_{12} + G_{13} \dot{C}_{22}
\end{aligned} \tag{C.13}$$

$$\begin{aligned}
\dot{H}_{12} = & \left(\frac{M}{c_1(2M-c_1)} n_1^3 n_2 - \frac{M}{c_2(2M-c_2)} n_1 n_2^3 - n_1 n_2 (n_1^2 - n_2^2) \frac{h_1-h_2}{c_1-c_2} \right) \dot{C}_{11} \\
& + \left(\frac{M}{c_1(2M-c_1)} 2n_1^2 n_2^2 + \frac{M}{c_2(2M-c_2)} 2n_1^2 n_2^2 + (n_1^2 - n_2^2)^2 \frac{h_1-h_2}{c_1-c_2} \right) \dot{C}_{12} \\
& + \left(\frac{M}{c_1(2M-c_1)} n_1 n_2^3 - \frac{M}{c_2(2M-c_2)} n_1^3 n_2 + n_1 n_2 (n_1^2 - n_2^2) \frac{h_1-h_2}{c_1-c_2} \right) \dot{C}_{22} \\
= & G_{21} \dot{C}_{11} + G_{22} \dot{C}_{12} + G_{23} \dot{C}_{22}
\end{aligned} \tag{C.14}$$

$$\begin{aligned}
\dot{H}_{22} = & \left(\frac{M}{c_1(2M-c_1)} n_1^2 n_2^2 + \frac{M}{c_2(2M-c_2)} n_1^2 n_2^2 - 2n_1^2 n_2^2 \frac{h_1-h_2}{c_1-c_2} \right) \dot{C}_{11} \\
& + \left(\frac{M}{c_1(2M-c_1)} 2n_1 n_2^3 - \frac{M}{c_2(2M-c_2)} 2n_1^3 n_2 + 2n_1 n_2 (n_1^2 - n_2^2) \frac{h_1-h_2}{c_1-c_2} \right) \dot{C}_{12} \\
& + \left(\frac{M}{c_1(2M-c_1)} n_2^4 + \frac{M}{c_2(2M-c_2)} n_1^4 + 2n_1^2 n_2^2 \frac{h_1-h_2}{c_1-c_2} \right) \dot{C}_{22} \\
= & G_{31} \dot{C}_{11} + G_{32} \dot{C}_{12} + G_{33} \dot{C}_{22}
\end{aligned} \tag{C.15}$$

where \dot{C}_{ij} , are the components of the material time derivatives of \mathbf{C} . The differential constitutive equation representing the FENE-P model is:

$$\dot{\mathbf{C}} = \mathbf{C} \cdot (\nabla \mathbf{u})^T + \nabla \mathbf{u} \cdot \mathbf{C} - \frac{1}{We} \left(\mathbf{I} - \frac{\mathbf{C}}{1 - \frac{\text{tr}(\mathbf{C})}{b^2}} \right) \tag{C.16}$$

Using Eq. (C.16) for the components of the material time derivative of \mathbf{C} and Eqs. (C.10)-(C.12) for the components of \mathbf{C} , the components of the material

time derivative of \mathbf{H} , \dot{H}_{ij} , defined by Eqs. (C.13)-(C.15) we derive

$$\dot{\mathbf{H}} = \frac{\partial \mathbf{H}}{\partial t} + (\mathbf{u} \cdot \nabla) \mathbf{H} = \begin{pmatrix} G_{11} & G_{12} & G_{13} \\ G_{21} & G_{22} & G_{23} \\ G_{31} & G_{32} & G_{33} \end{pmatrix} \left(\frac{\partial \mathbf{C}}{\partial t} + (\mathbf{u} \cdot \nabla) \mathbf{C} \right) \quad (\text{C.17})$$

which is used as the basis of the numerical algorithm for calculating the components of \mathbf{H} .

References

1. Afonso, A., Pinho, F., Alves, M.: The kernel-conformation constitutive laws. *Journal of Non-Newtonian Fluid Mechanics* **167-168**, 30 – 37 (2012)
2. Comminal, R., Spangenberg, J., Hattel, J.H.: Robust simulations of viscoelastic flows at high weissenberg numbers with the streamfunction/log-conformation formulation. *Journal of Non-Newtonian Fluid Mechanics* **223**, 37 – 61 (2015)
3. Coronado, O.M., Arora, D., Behr, M., Pasquali, M.: A simple method for simulating general viscoelastic fluid flow with an alternate log conformation formulation. *J. Non-Newtonian Fluid Mech.* **147**, 189–199 (2007)
4. Dupret, F., Marchal, J.M.: Loss of evolution in the flow of viscoelastic fluids. *J. Non-Newtonian Fluid Mech.* **20**(C), 143–171 (1986)
5. Fattal, R., Kupferman, R.: Constitutive laws for the matrix-logarithm of the conformation tensor. *J. Non-Newtonian Fluid Mech.* **123**, 281–285 (2004)
6. Fattal, R., Kupferman, R.: Time-dependent simulation of viscoelastic flow at high Weissenberg number using the log-conformation representation. *J. Non-Newtonian Fluid Mech.* **126**, 23–37 (2005)
7. Housiadas, K.D., Wang, L., Beris, A.N.: A new method preserving the positive definiteness of a second order tensor variable in flow simulations with application to viscoelastic turbulence. *Comput. Fluids* **39**(2), 225–241 (2010)
8. Hulsen, M.A.: A sufficient condition for a positive definite configuration tensor in differential models. *J. Non-Newtonian Fluid Mech.* **38**(1), 93–100 (1990)
9. Hulsen, M.A., Fattal, R., Kupferman, R.: Flow of viscoelastic fluid past a cylinder at high Weissenberg number: stabilized simulation using matrix logarithms. *J. Comput. Phys.* **127**, 27–39 (2005)
10. Jafari, A., Fiétier, N., Deville, M.O.: A new extended matrix logarithm formulation for the simulation of viscoelastic fluids by spectral elements. *Comput. Fluids* **39**(9), 1425–1438 (2010)
11. Kwon, Y.: Finite element analysis of planar 4:1 contraction flow with the tensor-logarithmic formulation of differential constitutive equations. *Korea-Australia Rheology J.* **4**, 183–191 (2004)
12. Kwon, Y., Leonov, A.I.: Stability constraints in the formulation of viscoelastic constitutive equations. *J. Non-Newtonian Fluid Mech.* **58**(1), 25–46 (1995)
13. Leonov, A.I.: Viscoelastic constitutive equations and Rheology for high-speed polymer processing. *J. Polym. Int.* **36**, 187–193 (1995)
14. Owens, R.G., Phillips, T.N.: *Computational Rheology*. Imperial College Press, London (2002)
15. Saramito, P.: On a modified non-singular log-conformation formulation for johnson-segalman viscoelastic fluids. *Journal of Non-Newtonian Fluid Mechanics* **211**, 16 – 30 (2014)
16. Tomé, M., Castelo, A., Afonso, A., Alves, M., Pinho, F.: Application of the log-conformation tensor to three-dimensional time-dependent free surface flows. *Journal of Non-Newtonian Fluid Mechanics* **175176**, 44 – 54 (2012)
17. Vaithianathan, T., Robert, A., Brasseur, J.G., Collins, L.R.: An improved algorithm for simulating three-dimensional, viscoelastic turbulence. *J. Non-Newtonian Fluid Mech.* **140**(1-3), 3–22 (2006)